Surface radiation balance in Antarctica as measured with automatic weather stations

Michiel van den Broeke, Carleen Reijmer, and Roderik van de Wal
Institute for Marine and Atmospheric Research, Utrecht University, Utrecht, Netherlands

Received 27 November 2003; revised 7 March 2004; accepted 15 March 2004; published 12 May 2004.

[1] We present 4 years of near-surface radiation balance observations of four Antarctic automatic weather stations (AWS). The AWS are situated along a traverse line in Dronning Maud Land, connecting the coastal ice shelf and the inland plateau via the katabatic wind zone, covering the three major climate regimes of East Antarctica. Important differences in the radiation balance of the three regions are found. Clouds not only limit atmospheric transmissivity for shortwave radiation but also strongly enhance the albedo for the shortwave radiation that reaches the surface. As a result, the snow surface of the coastal ice shelves absorbs up to 65% less shortwave radiation in high summer than at the high plateau, where cloudy episodes and precipitation events are less frequent. In winter, over the slopes, katabatic winds maintain a continuous turbulent transport of sensible heat toward the surface, which enhances outgoing longwave radiation. As a result, the katabatic wind zone shows the largest longwave and all-wave radiation loss in winter and over the year. Clear-sky effective emissivity for incoming longwave radiation shows great spatial variability resulting from differences in vertical temperature and moisture profiles among the various climate zones. *INDEX TERMS:* 3359 Meteorology and Atmospheric Dynamics: Radiative processes; 3394 Meteorology and Atmospheric Dynamics: Instruments and techniques; 3349 Meteorology and Atmospheric Dynamics: Polar meteorology; 3307 Meteorology and Atmospheric Dynamics: Boundary layer processes; 3309 Meteorology and Atmospheric Dynamics: Climatology (1620); *KEYWORDS:* polar meteorology, radiation balance, Antarctica

Citation: van den Broeke, M., C. Reijmer, and R. van de Wal (2004), Surface radiation balance in Antarctica as measured with automatic weather stations, *J. Geophys. Res.*, *109*, D09103, doi:10.1029/2003JD004394.

1. Introduction

[2] The surface radiation balance can be written as

$$\begin{aligned} R_{net} &= SHW_{net} + LW_{net} \\ &= SHW\downarrow + SHW\uparrow + LW\downarrow + LW\uparrow \\ &= SHW\downarrow\,(1-\alpha) + \varepsilon LW\downarrow - \varepsilon\sigma T_s^4, \end{aligned} \tag{1}$$

where fluxes toward the surface are defined as positive, R_{net} is the net radiation absorbed at the surface, SHW↓, SHW↑, LW↓, LW↑ are the downwelling and upwelling fluxes of shortwave and longwave radiation, α is the spectrally integrated surface albedo defined as $\alpha = -SHW\uparrow/SHW\downarrow$ (from now on just referred to as "albedo"), ε is the surface emissivity for longwave radiation, σ is the S. Boltzmann constant, and T_s is the surface temperature.

[3] At the snow surface that covers most of the Antarctic ice sheet, the radiation balance is extreme. Even in high summer solar zenith angles are large and the fine-grained, dry and clean snow surface absorbs only 5–25% of the incoming shortwave radiation [*Carroll and Fitch*, 1981]. On the other hand, snow, like most natural surfaces, has a high longwave emissivity ($\varepsilon \approx 0.98$ [*Wiscombe and Warren*, 1980]) so that it effectively looses heat in the form of longwave radiation. In combination with an atmosphere that is cold, dry, thin, clear and clean, this leads to a pronounced (longwave and all-wave) radiation deficit at the surface in winter. Compensating for this heat loss is an average turbulent transport of sensible heat from the atmosphere to the surface. This makes the Antarctic ice sheet a major heat sink in the Earth's atmosphere and introduces a strong coupling between the radiation balance and near-surface climate [*Dutton et al.*, 1991; *Stanhill and Cohen*, 1997].

[4] To get a good grip on the surface radiation balance of the Antarctic ice sheet, accurate observations are needed. However, keeping radiation sensors free of snow and rime requires continuous heating and ventilation of the sensors so that accurate, year-round measurements of the surface radiation balance can only be made at manned stations. At present, three Antarctic stations are part of the Baseline Surface Radiation Network (BSRN) [*Ohmura et al.*, 1998]: Neumayer, Syowa and South Pole (Figure 1). Other radiation observations in Antarctica have been made during dedicated meteorological experiments [*Liljequist*, 1957; *Schlatter*, 1972; *Kuhn et al.*, 1977; *Weller*, 1981; *Ohata et al.*, 1985a; *Wendler et al.*, 1988; *King et al.*, 1989; *Bintanja*

Copyright 2004 by the American Geophysical Union.
0148-0227/04/2003JD004394$09.00

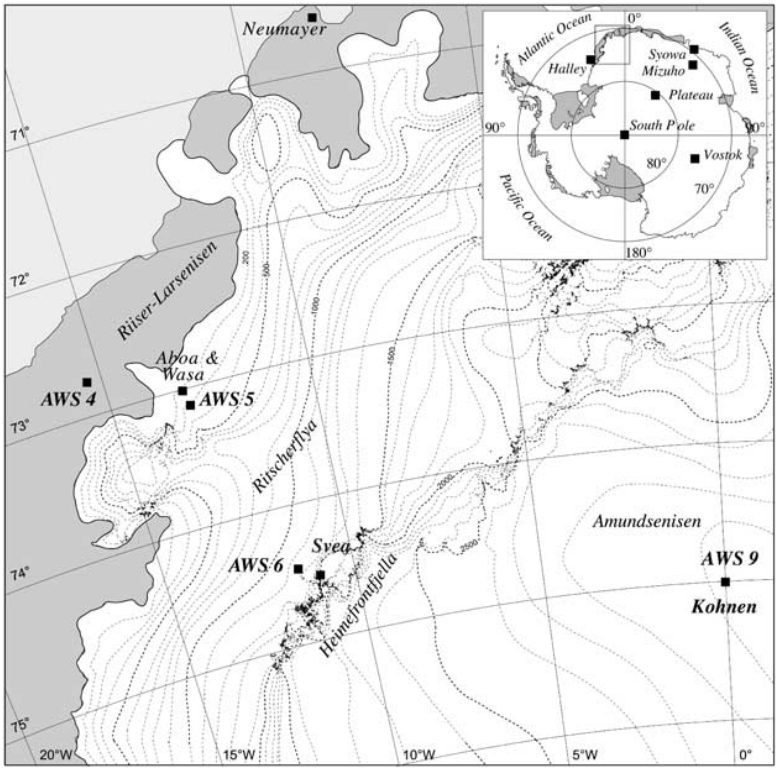

Figure 1. Map of western Dronning Maud Land, Antarctica, with AWS locations, main topographical features, ice shelves (grey), height contours (dashed lines, height interval 100 m), and station locations.

and van den Broeke, 1995; *Walden et al.*, 1998; *Bintanja*, 2000; D. van As et al., The surface energy balance of the high Antarctic Plateau in summer, submitted to *Boundary-Layer Meteorology*, 2004].

[5] The problem of poor data coverage in time and space can be partly remedied by the use of automatic weather stations (AWS). AWS have been used successfully to monitor the climate of inland Antarctica [*Stearns and Wendler*, 1988; *Stearns et al.*, 1993; *Allison et al.*, 1993; *Renfrew and Anderson*, 2002] as well as other remote glaciated regions. In 1997–1998, an array of AWS was installed in western Dronning Maud Land (Figure 1), equipped with Kipp & Zonen CNR1 radiation sensors that separately measure the four radiation components SHW↓, SHW↑, LW↓ and LW↑ (Figures 2a and 2b). In this paper we present 4 years of AWS radiation data, expanding on results presented previously by *Reijmer* [2001] and *Reijmer and Oerlemans* [2002]. In section 2 we describe the experimental setup and data treatment methods, followed by results in section 3, discussion in section 4, and a summary in section 5.

2. Methods

2.1. AWS Site Description

[6] The AWS are situated in western Dronning Maud Land (DML), East Antarctica, along a traverse line connecting in a southeasterly direction the coastal ice shelf (AWS 4) to the polar plateau (AWS 9) via the katabatic wind zone (AWS 5 and 6) (Figure 1). These represent the three major climate regimes in East Antarctica [*van den Broeke et al.*, 2002]. Around the AWS, in an area with a radius of at least several kilometers, the surface consists of undisturbed snow. A short description of the AWS sites is given below:

[7] AWS 4 (72°45.2′S, 15°29.9W, 34 m asl) is located on the flat Riiser-Larsen ice shelf some 80 km away from the ice shelf front and 40 km from the grounding line. The ice shelf slopes seaward with a rate of typically 0.1 m km^{-1}.

[8] AWS 5 (73°06.3′S, 13°09.9W, 363 m asl) is located just inland of the grounding line, on the coastal slopes of the ice sheet. The estimated large-scale surface slope at AWS 5 is 13.5 m km^{-1}.

[9] AWS 6 (74°28.9′S, 11°31.0W, 1160 m asl) is situated at the foot of the Heimefront Mountains in the katabatic wind zone, where the large-scale surface slope is approximately 15 m km^{-1}.

[10] AWS 9 (75°00.2′S, 0°00.4E, 2892 m asl) is situated on Amundsenisen on the East Antarctic plateau, where the estimated large-scale surface slope is about 1.3 m km^{-1}.

[11] A picture of AWS 9 is given in Figure 2a. Apart from atmospheric radiation, the AWS measure snow temperatures at various depths and basic meteorological variables like wind speed and direction, temperature, relative humidity, sensor height and air pressure. Most variables, including radiation, are sampled at 6-min intervals (instantaneous, except for wind speed, cumulative) after which 2-hour averages are stored in a Campbell CR10 datalogger with separate memory module.

2.2. Description of the Radiation Sensor

[12] The AWS are equipped with a Kipp & Zonen (K&Z) CNR1 net radiometer (Figure 2b). This sensor houses two

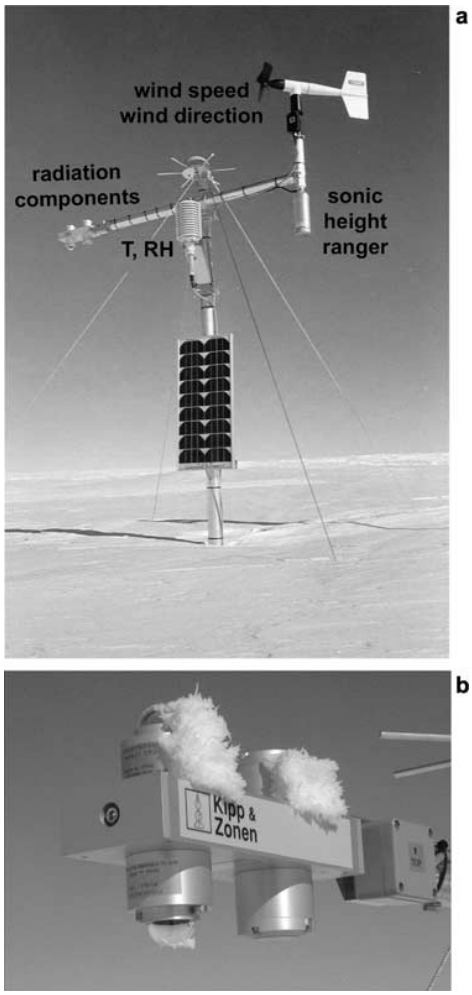

Figure 2. (a) Picture of AWS 9, taken 4 years after installation, i.e., after approximately 1 m of snow has accumulated. The datalogger and pressure sensor are buried in the snow. The other AWS have similar designs. (b) Enlargement of radiation sensor with ice accretion. See color version of this figure at back of this issue.

K&Z CM3 pyranometers for downward and upward broadband shortwave radiation flux (spectral range 305–2800 nm) and two K&Z CG3 pyrgeometers for downward and upward broadband longwave radiation flux (spectral range 5–50 μm). The K&Z CM3 pyranometer is a thermopile type pyranometer, covered by a single glass dome, which complies with ISO 9060 second-class specifications (estimated accuracy for daily totals ±10%). The K&Z CG3 pyrgeometer consists of a thermopile sensor covered by a silicon window that is transparent for far-infrared radiation but absorbs solar radiation. No international standard exists for pyrgeometers; the factory-provided estimated accuracy of the K&Z CG3 for daily totals is also ±10%.

[13] Before and during deployment, the sensors have been compared to higher standard sensors and were found to have very stable calibration constants that did not drift in time. For instance, *van den Broeke et al.* [2004b] compared radiation measurements of the K&Z CNR1 with radiation data collected at Neumayer station, a BSRN station (70.7°S, 8.4°W, 50 m asl) for a 10-day period in February 2001. At Neumayer, the radiation instruments (K&Z CM11 for shortwave radiation and Eppley PIR for longwave radiation) are ventilated with slightly heated air to prevent rime formation. The comparison yielded a root mean square difference of 2.7% (4.8 W m^{-2}) for daily mean SHW↓ and 1.2% (2.7 W m^{-2}) for daily mean LW↓. This shows that under controlled conditions the K&Z CM3 and CG3 perform much better than the listed specifications. For more detailed information on this and two other Antarctic radiation comparison experiments, the reader is referred to *van den Broeke et al.* [2004b].

2.3. Data Treatment: Shortwave Radiation

[14] In spite of the good performance of the individual sensor components, problems may occur when external factors affect the measurements or when different signals are combined, for instance to calculate a net radiation flux. The study by *van den Broeke et al.* [2004b] signals two serious problems in the AWS radiation data from Antarctica. The first problem concerns the calculation of SHW_{net}. Because the upward facing K&Z CM3 receives direct radiation, the (clear-sky) measurement of SHW↓ is much more sensitive than SHW↑ to errors associated with ice accretion, rime formation, low Sun angle (poor cosine response) and sensor tilt. As a result, when SHW_{net} is calculated from individual pairs of SHW↓ and SHW↑, the absolute error in SHW↓ is directly introduced in SHW_{net}. The latter being small over a highly reflective surface (α = 0.8–0.9), the relative error in SHW_{net} becomes in the order of 25%. Using SHW↑ as the basis for the calculation of SHW_{net} solves this problem. This is made possible by introducing the "accumulated albedo" α_{acc}, which is defined as the ratio of values of SHW↓ and SHW↑ that have been accumulated over a time window of 24 hours, centered around the moment of observation. The α_{acc} is then used together with instantaneous SHW↑ to calculate instantaneous SHW_{net}. The basic underlying assumption for this idea is that changes in α due to snow metamorphism are small on a subdaily timescale. An additional advantage of this method is that riming/icing events can be easily detected and corrected by prescribing lower and upper bounds for α_{acc} (in this paper we used 0.75 and 0.95, respectively). As we will see later, these values are seldom reached and icing/riming of the K&Z CM3 is not considered a serious problem during summer, thanks to its single glass dome [*van den Broeke et al.*, 2004b]. An obvious disadvantage of the method is that the clear-sky daily cycle in α is eliminated. This is remedied by adding a theoretical daily cycle for a semi-infinite snow pack to the "clear-sky" part of α_{acc} [*Wiscombe and Warren*, 1980]. For more detail the reader is referred to *van den Broeke et al.* [2004b].

2.4. Data Treatment: Longwave Radiation

[15] A serious problem that affects 25–30% of the measurements of LW↓ at AWS 4 and 9 is the formation of rime in winter on the upward looking sensor window. This rime coating completely obstructs the transmission of longwave radiation and leads to serious overestimation of LW↓ under clear-sky conditions. The only way to obtain useful estimates of LW↓ during these periods is to use

Table 1. AWS Topographic and Climate Characteristics, 1998–2001[a]

	AWS 4	AWS 5	AWS 6	AWS 9
Start of observation	22 Dec. 1997	3 Feb. 1998	15 Jan. 1998	1 Jan. 1998
End of observation	21 Dec. 2001	2 Feb. 2002	14 Jan. 2002	31 Dec. 2001
Elevation, m asl	34	363	1160	2892
Surface slope, m km^{-1}	0.1	13.5	15.0	1.3
SSMB, kg m^{-2} yr^{-1}	393	179	267	74
Temperature, K	254.3	256.8	252.6	230.0
Potential temperature, K	255.9	261.3	264.3	257.1
Relative humidity, %	93	83	78	93
Specific humidity, g kg^{-1}	1.03	1.01	0.72	0.17
10 m wind speed, m s^{-1}	5.7	7.8	7.7	4.8

[a]If no height is specified, the mean value at AWS sensor level is used. SSMB, specific surface mass balance. The 10 m wind speed was obtained through flux-profile relations.

parameterized values of LW↓ based on surface temperature and time of year. This yields an uncertainty in daily mean LW↓ of 10–15 W m^{-2} but removes the systematic overestimation of LW↓ [*van den Broeke et al.*, 2004b]. In the following, it will be clearly indicated for which periods this approach was used.

[16] Icing also occurs on the downward looking sensor window, but this problem is less serious because sensor and snow surface temperatures are similar. Nevertheless, during these periods we calculate LW↑ using a surface temperature obtained from a full energy balance calculation.

3. Results

3.1. General Meteorological Conditions

[17] Table 1 lists basic climate information for the four AWS sites. All four AWS are situated in net accumulation areas with a positive specific surface mass balance ranging from 74 at AWS 9 to 393 kg m^{-2} yr^{-1} at AWS 4 (M. R. van den Broeke et al., A study of the surface mass balance in Dronning Maud Land, Antarctica, using automatic weather stations, submitted to *Journal of Glaciology*, 2004) (hereinafter referred to as van den Broeke et al., submitted manuscript, 2004). With the locally measured density of the surface snow (300–330 kg m^{-3}) this corresponds to 25 and 98 cm of snow accumulation each year. The highest annual mean surface temperature occurs at AWS 5, in spite of the fact that this station is situated about 330 m higher than AWS 4. The reason is that the surface at AWS 5 and 6 has a significant slope, which forces katabatic winds that mix relatively warm air downward to the surface, which results in elevated surface (potential) temperatures [*Bromwich*, 1989; *King et al.*, 1998; *van den Broeke et al.*, 1999]. As we will see later, this directly influences the longwave radiation balance at the surface (section 3.3).

[18] The influence of the katabatic winds is also visible in the higher mean wind speed and lower relative humidity at AWS 5 and 6, promoting surface sublimation. High temperatures and sublimation rates enhance surface snow metamorphosis (grain growth). This indirectly influences the summertime shortwave radiation balance through the surface albedo (next section). Situated on the high and relatively flat Antarctic plateau, AWS 9 has a very cold climate with relatively weak winds, high relative humidity and extremely low absolute air moisture content. Precipitation events are rare, except at AWS 4, and they seldom deposit more than a few centimeters of fresh snow [*Reijmer and van den Broeke*, 2004].

3.2. Shortwave Radiation

[19] Figures 3a–3d show daily mean values of incoming shortwave radiation at the top-of-atmosphere (TOA) and at the surface (SHW↓ and SHW_{net}), Figures 4a–4d show daily means of α_{acc} and Figures 5a–5c show the mean seasonal cycles through monthly averages. Table 2 lists annual mean values of the radiation fluxes and derived variables. We included in addition data of Neumayer in Table 2 (data available from http://www.awi-bremerhaven.de); Neumayer is situated on Ekstrømisen, an ice shelf some two latitudinal degrees north and eight longitudinal degrees east of AWS 4 (Figure 1).

3.2.1. Incoming Shortwave Radiation

[20] High interdiurnal variability of SHW↓ at the coastal sites AWS 4 and 5 (Figures 3a and 3b) is indicative of the frequent passage of frontal systems and associated clouds. In spite of the highest TOA radiation, AWS 4 has the lowest annual mean SHW↓ (Table 2), which also holds for each individual nonwinter month (Figure 5a). At this coastal site, not only is more shortwave radiation scattered and absorbed in the relatively thick atmosphere, clouds are also more abundant this close to the sea, as is fog; this results in a mean atmospheric transmissivity for shortwave radiation ($SHW\downarrow/SHW_{TOA}$) of 0.64 at AWS 4, similar to the value for Neumayer (Table 2). Transmissivity for shortwave radiation increases to 0.79 at AWS 9, a change of 25% compared to AWS 4. The decreasing influence of clouds toward the interior is also visible by the strongly reduced interdiurnal variability in SHW↓ at AWS 6 and 9 (Figures 3c and 3d).

3.2.2. Albedo

[21] Because of its relatively great air content, dry Antarctic snow conducts heat poorly so surface temperature adjusts rapidly to changes in the surface radiation balance. That is why the albedo is of great importance for the summertime surface energy budget. The albedo α of a semi-infinite clean and dry snow pack depends mainly on cloud cover, grain size (snow age) and solar zenith angle [*Wiscombe and Warren*, 1980]. Clouds make solar radiation reaching the surface more diffuse, which decreases α for solar zenith angles >50° (typical for Antarctica). However, they also make SHW↓ relatively richer in visible wavelengths, enhancing α. We found that in Antarctica the latter effect dominates. Snow metamorphosis is slow in the cold and dry Antarctic snow, which has a relatively small grain

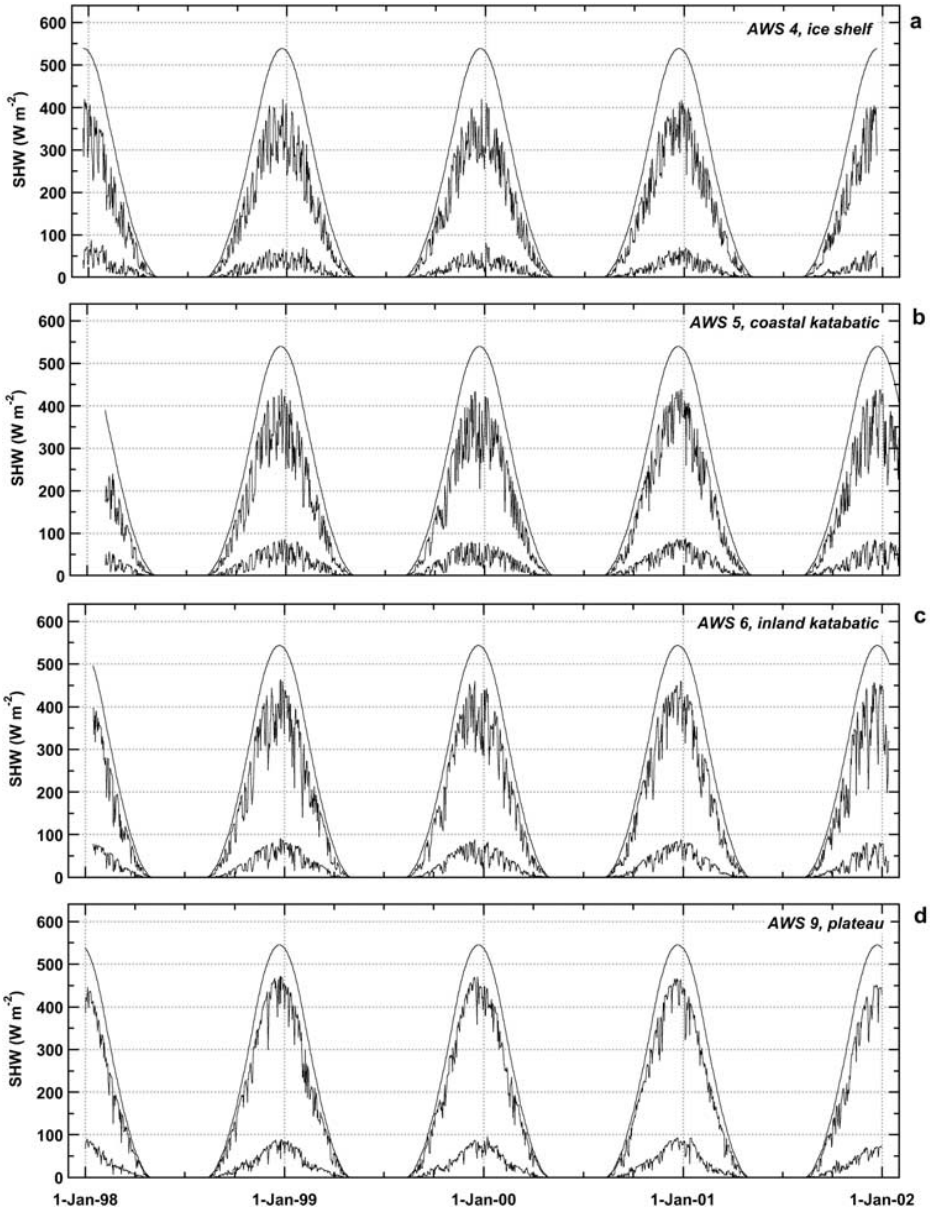

Figure 3. Daily mean values of TOA (upper curve) and near-surface incoming (middle) and net shortwave radiation (lower curve), 1998–2001, at (a) AWS 4, (b) AWS 5, (c) AWS 6, and (d) AWS 9.

size of typically 0.1 mm [*Gay et al.*, 2002], which leads to high values of α. The speed at which snow grains grow depends primarily on temperature [*Colbeck*, 1975] and will thus be faster in the coastal regions where temperatures are relatively high. A third important factor influencing (clear-sky) values of α is solar zenith angle; in the absence of effects due to metamorphosis and clouds, this would force a seasonal cycle of daily mean α with maxima in early and late summer.

[22] The daily mean values of α_{acc} in Figures 4a–4d in excess of 0.9 occur during precipitation events (thick clouds, fresh snow). AWS 4 has the greatest frequency of cloud and significant precipitation events [*Reijmer and van den Broeke*, 2004], and daily mean α_{acc} seldom falls below 0.8 and regularly exceeds 0.9 (Figure 4a). The annual α_{acc} values listed in Table 2 range from 0.84 at AWS 5 to 0.88 at AWS 4. The annual mean α_{acc} at AWS 4 (0.88) and Neumayer (0.85) are among the highest values reported in literature.

[23] AWS 5 is the warmest of the four AWS and the driest of the nonplateau AWS (Table 1). Advanced metamorphosis of the surface snow or the surfacing of old snow layers after extended periods of surface sublimation (van den Broeke et al., submitted manuscript, 2004) regularly enables daily mean α_{acc} values as low as 0.78 (Figure 4b). At AWS 6, α_{acc} is somewhat higher than at AWS 5, which reflects the more positive surface mass balance at AWS 6 compared to AWS 5 (Table 1); AWS 6 is situated at the foot of the Heimefrontfjella, which triggers orographic precipitation. At AWS 6 and especially at AWS 9, clouds become

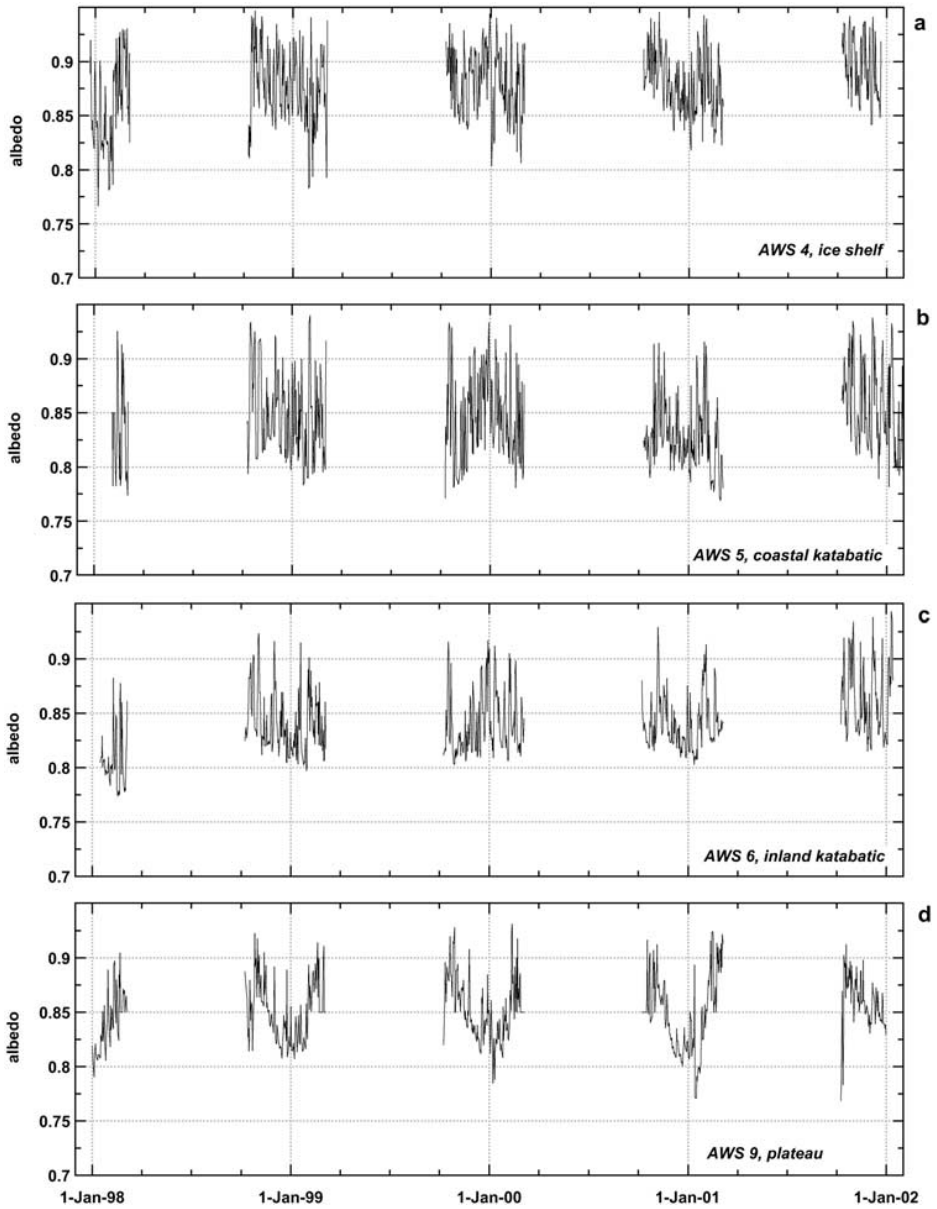

Figure 4. Daily mean values of accumulated albedo α_{acc} at (a) AWS 4, (b) AWS 5, (c) AWS 6, and (d) AWS 9. Days are included with mean solar zenith angle < 0.8.

optically thinner and occur less frequently, which results in smaller interdiurnal variability of α_{acc} (Figures 4c and 4d).

[24] At AWS 9, clear-sky conditions prevail, and the very low temperatures make snow grain grow very slowly. With little influence of cloud cover and snow metamorphosis, α_{acc} mainly responds to variations in solar zenith angle resulting in a minimum α_{acc} in the middle of summer (Figures 4d and 5b). At AWS 4 and 5, a declining albedo trend is visible throughout the summer (Figure 5b), most likely driven by progressing snow metamorphosis at these relatively warm coastal sites. AWS 6 appears to be a transition site from the coastal albedo regime with a declining trend to the plateau with its midsummer minimum.

3.2.3. Net Shortwave Radiation

[25] While absolute differences in α_{acc} between the AWS are small, the absorbed fractions $(1 - \alpha_{acc})$ show great relative differences; for instance, $(1 - \alpha_{acc})$ at AWS 5 is 30% greater than at AWS 4. The result is that the coastal ice shelves absorb considerably less shortwave radiation in summer than do other parts of Antarctica, which makes them more sensitive to feedback mechanisms that involve surface albedo, like melting. This is of special interest in view of the recent catastrophic disintegration of ice shelves in the northern Antarctic Peninsula, which is believed to be related to enhanced surface melting in summer [*Vaughan and Doake*, 1996].

[26] Annual mean SHW_{net} at AWS 4 is 15.4 W m^{-2}, which represents only 8.0% of TOA (Table 2). In contrast, SHW_{net} at AWS 9 is 22.6 W m^{-2} (12.1% of TOA). On an annual basis, the snow surface at AWS 9 receives 47% more energy in the form of solar radiation than at AWS 4. Daily means of SHW_{net} at AWS 4

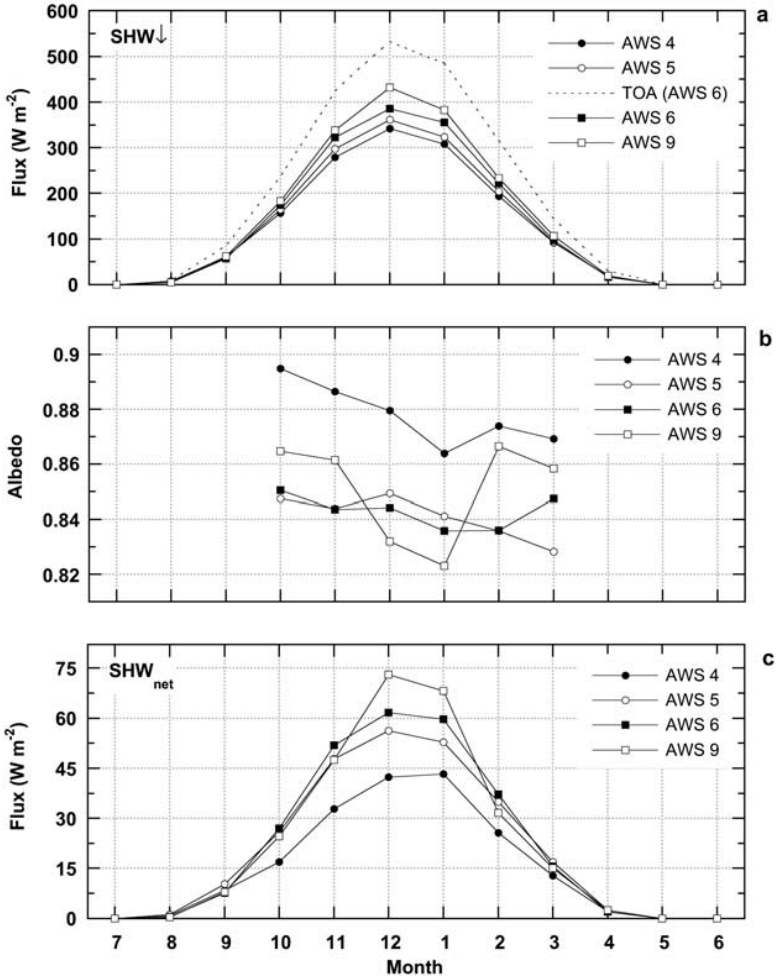

Figure 5. Average monthly mean values of (a) incoming shortwave radiation, (b) albedo, and (c) net shortwave radiation.

seldom exceed 60 W m^{-2} while peaks near 100 W m^{-2} are reached at the other AWS (Figures 3a–3d). In midsummer, thick clouds may reduce daily mean SHW_{net} at AWS 4 to less than 20 W m^{-2}, while at AWS 9 this seldom drops below 50 W m^{-2}. The differences in SHW_{net} between ice shelf and plateau peak in high summer (Figure 5c): In December and January combined, the surface at AWS 9 absorbs 65% more shortwave radiation than at AWS 4.

3.3. Longwave Radiation

[27] Results for LW↓ and LW_{net} are presented in Figures 6–8 and Table 2. Figures 6a–6e show scatterplots of LW_{net} vs. surface temperature. The light grey dots

Table 2. Annual Mean Radiation Fluxes and Derived Parameters for the 4-Year Period Indicated

	AWS 4	AWS 5	AWS 6	AWS 9	Neumayer
Start of observation	22 Dec. 1997	3 Feb. 1998	15 Jan. 1998	1 Jan. 1998	1 Jan. 1998
End of observation	21 Dec. 2001	2 Feb. 2002	14 Jan. 2002	31 Dec. 2001	31 Dec. 2001
SHW↓	121.3	127.2	136.0	146.7	126.0
SHW↑	−105.9	−106.5	−114.1	−124.1	−106.8
SHW_{net}	15.4	20.7	21.9	22.6	19.2
LW↓	212.2	204.8	180.2	125.4	215.8
LW↑	−234.6	−241.1	−224.2	−154.9	−244.9
LW_{net}	−22.4	−36.3	−44.0	−29.5	−29.1
R_{net}	−7.0	−15.6	−22.1	−6.9	−9.9
TOA	191.8	191.1	188.3	187.3	196.1
α_{acc}	0.877	0.840	0.843	0.850	0.848
|SHW↑/SHW↓|	0.873	0.837	0.839	0.846	0.848
SHW↓/TOA	0.632	0.666	0.722	0.783	0.642
SHW_{net}/TOA	0.080	0.108	0.116	0.121	0.098

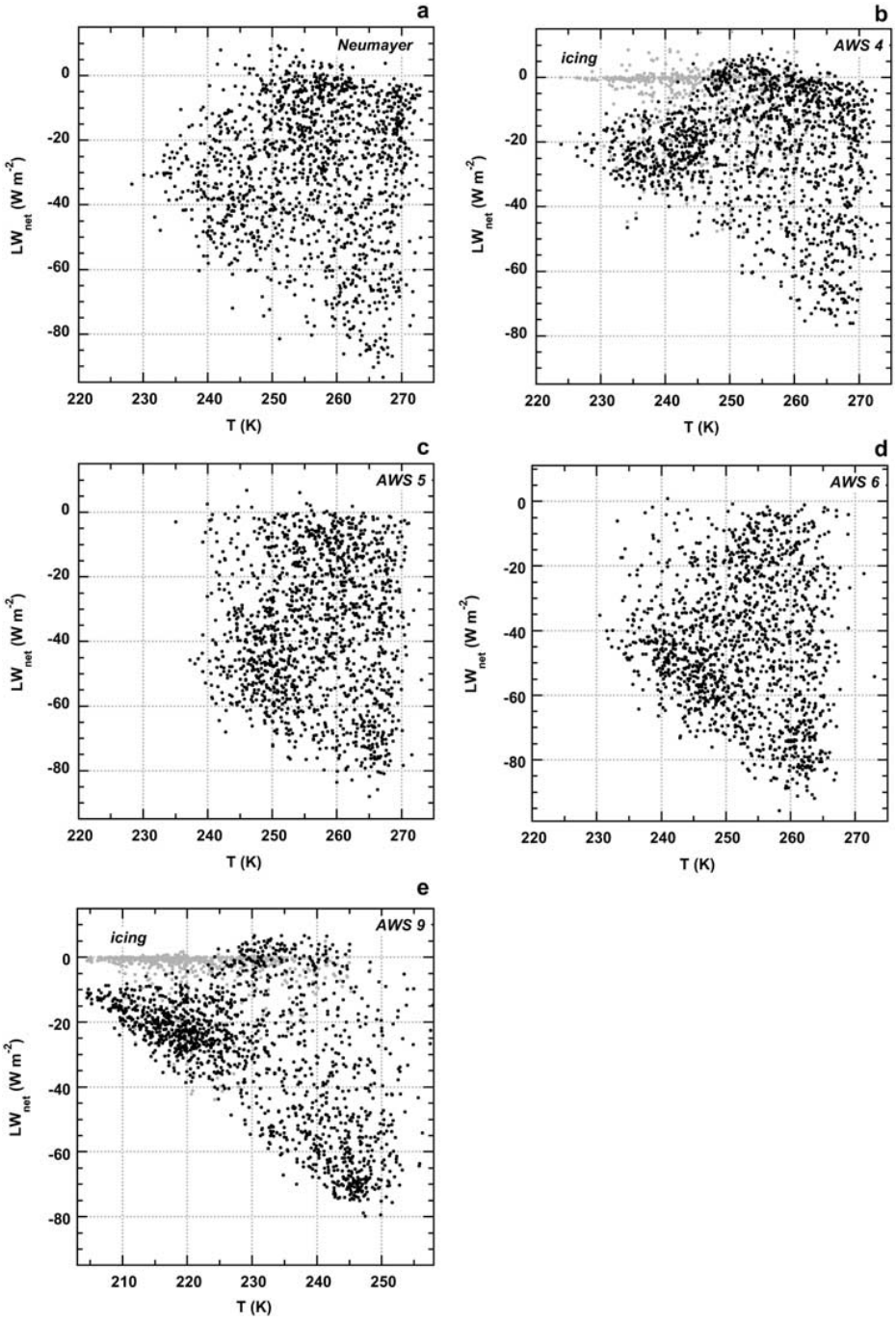

Figure 6. Daily mean values of net longwave radiation as a function of AWS temperature, 1998–2001, at (a) Neumayer, (b) AWS 4, (c) AWS 5, (d) AWS 6, and (e) AWS 9. The grey dots represent measurements that are rejected because of riming problems.

represent measurements that have been replaced by parameterized values because of suspected riming. Figures 7a–7d show daily mean time series of LW↓ and LW_{net}. Rejected LW↓ data are plotted as dashed lines. Figures 8a–8c show the average annual cycle, based on monthly means, and Table 2 lists annual mean values.

3.3.1. Temperature Dependence of LW_{net}

[28] Under clear-sky conditions, there is a strong link between LW↓ and LW↑ (i.e., near-surface temperature; *König-Langlo and Augstein* [1994] and *King* [1996]). Under cloudy conditions, LW↓ is mainly sensitive to cloud base temperature. Much can be learned by considering LW_{net} as a function of near-surface T (Figures 6a–6e). For all four AWS, $LW_{net} = 0$ is a clear upper boundary; this represents cloudy conditions during which the snow surface thermally equilibrates with the cloud base, both radiating at similar temperatures. An example is warm air intrusions during winter ($SHW_{net} = 0$), when

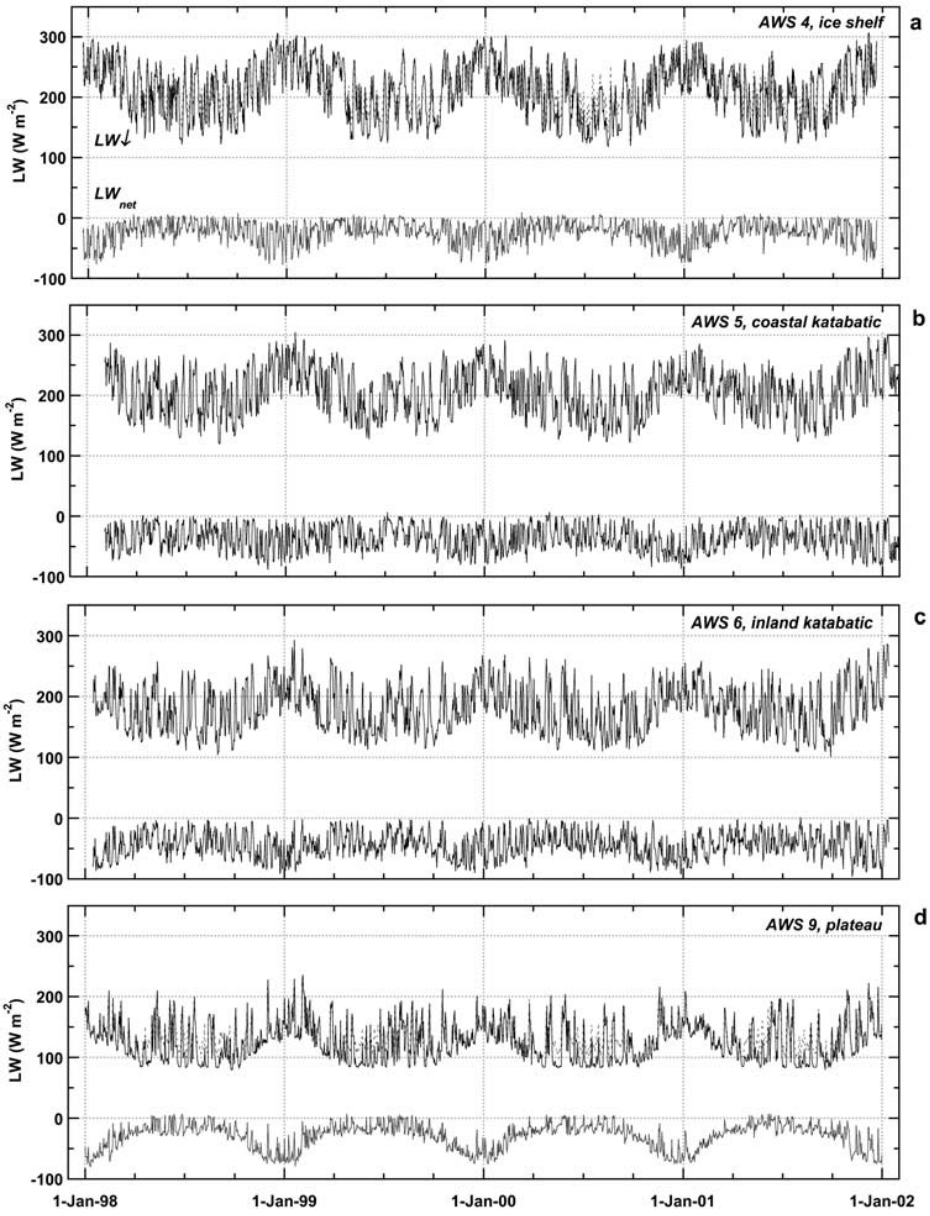

Figure 7. Daily mean values of near-surface incoming (upper line) and net longwave radiation (lower line), 1998–2001, at (a) AWS 4, (b) AWS 5, (c) AWS 6, and (d) AWS 9. Dashed lines represent measurements that have been replaced with parameterized values because of riming problems.

small vertical temperature gradients imply small vertical sensible heat and moisture fluxes.

[29] The lower, sloping boundary of the point clouds in Figures 6a–6e represents clear-sky conditions, when LW_{net} is negative and at a minimum for a given temperature. Longwave radiative heat loss during clear-sky conditions is greatest in summer, when absorption of shortwave radiation warms the snow surface, resulting in more negative LW↑ and LW_{net}. In the absence of solar radiation, other heat sources (usually sensible heat transport) must compensate for the surface longwave radiative loss under clear-sky conditions.

[30] In theory, however, when all other surface heat fluxes are small, LW↓ and LW↑ can also balance under clear-sky conditions. The (theoretical) value of T at which LW↓ and LW↑ balance represents a climatological temperature minimum for a particular site and is represented by the intersection of the lower and upper LW_{net} envelopes in Figures 6a–6e. Fitting straight lines through the 5th and 95th percentiles of daily mean LW_{net} collected in 5 K T bins yields values of 206 K and 190 K for AWS 4 and 9, respectively. As can be seen, these conditions are never entirely met: The reason is that when T becomes very low, large near-surface temperature gradients within the snow force a significant subsurface heat flux from the deeper, warmer snow layers toward the surface, which partly compensates the longwave radiative energy loss.

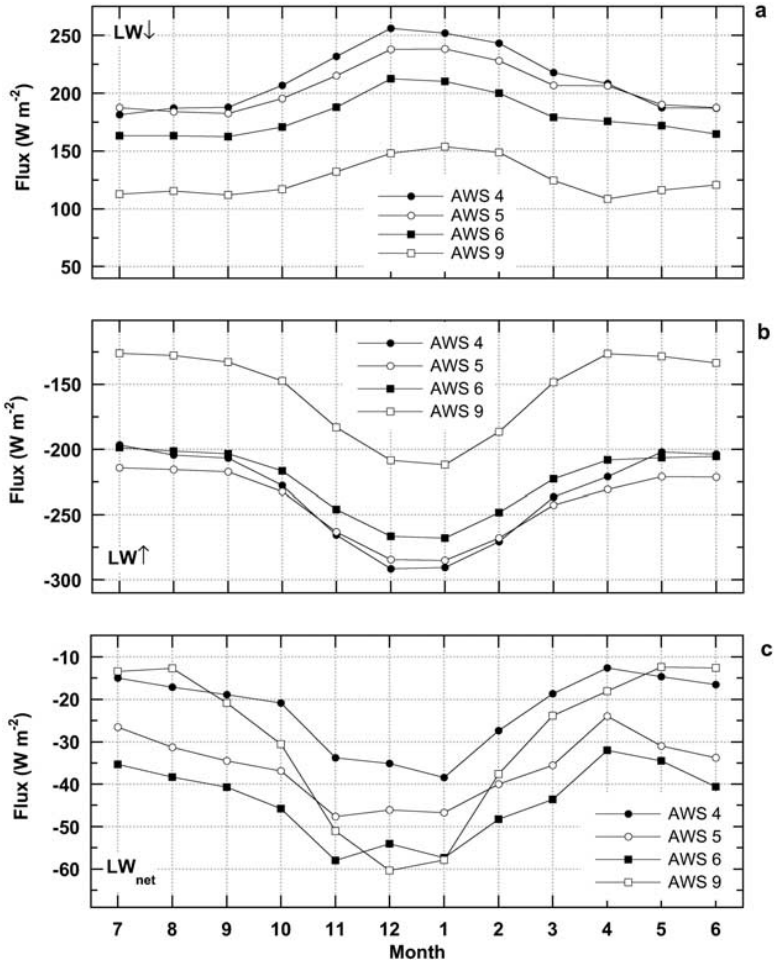

Figure 8. Average monthly mean values of (a) incoming longwave radiation, (b) outgoing longwave radiation, and (c) net longwave radiation.

[31] At AWS 5 and 6, the combination of low T and modestly negative LW_{net} does not occur; that is, the triangular data cloud in Figures 6c and 6d misses the upper left corner. Being situated on a slope, these AWS experience persistent katabatic winds in winter that maintain a continuous flow of sensible heat toward the surface, enhancing T_s and thus LW↑, keeping LW_{net} strongly negative. This explains the relatively high annual mean T_s and large longwave radiation deficit at AWS 5 and 6 (Table 2).

[32] Longwave radiative heat loss is the most significant surface heat sink in winter; low wintertime T_s in Antarctica thus require a negative LW_{net}. The clustering of light grey (rejected) data points around $LW_{net} = 0$ at low T_s at AWS 4 (Figure 6b) and AWS 9 (Figure 6e) represent measurement errors related to icing of the LW↓ sensor. As stated in section 2.3, these erroneous LW↓ measurements at AWS 4 and 9 have been replaced by parameterized values in order to be able to calculate monthly and annual means. Riming does not occur either at Neumayer (Figure 6a), where the sensors are ventilated, or at AWS 5 and 6 (Figures 6c and 6d), where katabatic winds promote sublimation even in winter so that the sensors remain ice-free.

3.3.2. Interdiurnal and Seasonal Variability of Longwave Radiation Fluxes

[33] At all four AWS, LW↓ shows very large interdiurnal variability of 120–140 W m^{-2} due to alternating clear and cloudy episodes (Figures 7a–7d). Cloudy days are more frequent at the coastal stations AWS 4 and 5 while clear-sky conditions prevail at AWS 9. Because T_s and hence LW↑ reacts quickly to changes in LW↓, a strong correlation exists between daily means of LW↓ and LW↑ (R = 0.8 to 0.9, not shown). As a result, interdiurnal variability in LW_{net} is smaller at 30–80 W m^{-2} (Figures 7a–7d, lower lines). Variability in LW_{net} is greatest in summer at AWS 5 and 6 and smallest in winter at AWS 9, although the latter may be partly caused by the less dynamic behavior of the parameterized LW↓.

[34] The interdiurnal variability in LW↓ is superimposed on a seasonal cycle (Figure 8a) with a range of 40 W m^{-2} (AWS 9) to 70 W m^{-2} (AWS 4). The greater annual cycle at AWS 4 is probably caused by the nonlinear response of air moisture content with temperature, causing an annual cycle

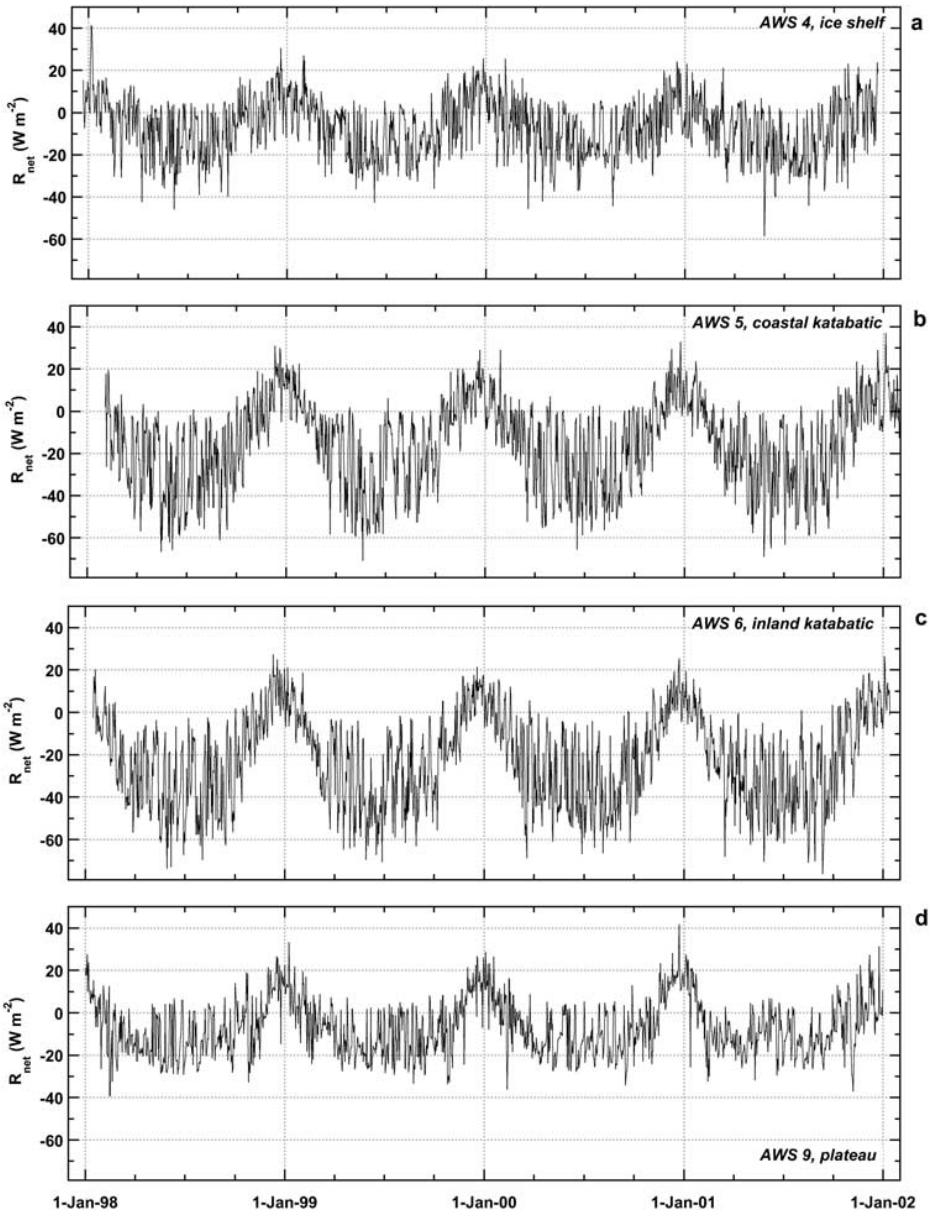

Figure 9. Daily mean values of near-surface net all-wave radiation, 1998–2001, at (a) AWS 4, (b) AWS 5, (c) AWS 6, and (d) AWS 9.

in atmospheric (clear-sky) emissivity that is greater near the coast than inland. The seasonal cycle of LW↑ (Figure 8b) reflects the annual cycle of T_s, which has the greatest amplitude at AWS 9; this is associated with the formation of a strong surface temperature inversion on the plateau in winter and its removal in summer under influence of shortwave radiation absorption. The seasonal cycle of LW_{net} is also greatest at AWS 9. Note that in the annual mean, both LW components have magnitudes greater than their SHW counterparts, except for the incoming fluxes at AWS 9 (Table 2).

3.4. Net Radiation

[35] Figures 9a–9d show daily mean $R_{net} = SHW_{net} + LW_{net}$ at the four AWS and Figure 10 presents the average seasonal cycle based on monthly means. At all four AWS, R_{net} is negative to zero in winter and slightly positive in December and January. Because SHW_{net} and LW_{net} are strongly coupled, the interdiurnal variability of R_{net} is smallest in summer. From month to month, R_{net} is most negative in the katabatic wind zone at AWS 6 (Figure 10); averaged over the year, this results in a mean radiative heat loss at AWS 6 of 22.1 W m^{-2}, more than three times as much as the values found at AWS 4 and 9 (Table 2). This heat sink is mainly compensated by a transport of sensible heat from the air to the surface.

4. Discussion

4.1. Comparison With Other Stations

[36] *King and Connolley* [1997] and *King and Turner* [1997] compiled monthly mean radiation data from various

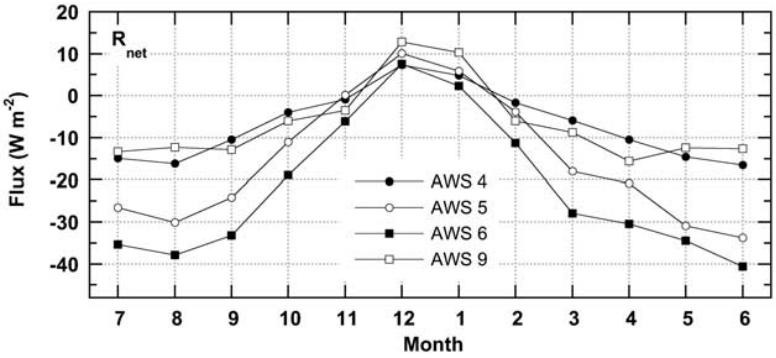

Figure 10. Average monthly mean values of net all-wave radiation.

Antarctic sites. Table 3 compares these data with our results for typical summer (December/January) and winter (July/August) conditions as well as for the year. A direct comparison is difficult, because the periods of observation do not overlap and sometimes cover only one year (Plateau station, Syowa). Some general statements can however still be made. The four plateau stations have very similar values for albedo and summer SHW_{net}. These values agree with those listed by *Carroll and Fitch* [1981], adapted from *Kuhn et al.* [1977]. However, summer LW_{net} at Vostok is relatively high, and as a result, summer R_{net} at Vostok is also higher than at the other stations. No direct explanation is available for this. Annual R_{net} is weakly negative at all plateau sites.

[37] In the inland katabatic wind zone, the winter longwave balances of AWS 6 and Mizuho are similar. Important differences show up in summer. At Mizuho, the combination of a dry climate due to its high elevation (2200 m asl) and strong wintertime katabatic winds and associated sublimation (July/August mean 14 m s^{-1} [*Ohata et al.*, 1985b]) give the snow surface a glazed character [*Fujii and Kusunoki*, 1982]. The albedo of this highly metamorphosed surface with large ice crystals is relatively low, 0.78 [*Ohata et al.*, 1985a], which causes summertime SHW_{net} at Mizuho to be 30% greater than at AWS 6. The relatively high surface temperature that results from the enhanced absorption of solar radiation also leads to a stronger longwave radiation loss. The net result is that summer R_{net} at Mizuho is about three times that of AWS 6, and similar to the values found at the plateau stations (Table 3). AWS 6 combines a high albedo with moderate katabatic winds, and as a result has the strongest negative annual R_{net} of all stations under consideration.

[38] In the coastal zone, a similar difference between Syowa and AWS 5 is found. Syowa, like Mizuho, has a relatively low albedo of 0.74 [*Yamanouchi and Ørbaek*, 1995]. As a result, summer SHW_{net} is 50% greater and R_{net} about three times as large as at AWS 5. Wintertime LW_{net} at Syowa is comparable to values found at Mawson (-43 W m^{-2} [*Weller*, 1981]) but significantly more negative than at AWS 5. No direct explanation is available. While Mawson experiences very strong wintertime katabatic winds (July/August mean of 12 m s^{-1} [*Streten*, 1990]), wintertime wind speeds at offshore Syowa are more moderate and comparable to AWS 5 (about 8 m s^{-1}). Cloud cover is an obvious other candidate; the average July/August cloud cover at Syowa and Mawson are similar (63% and 70% [*Schwerdtfeger*, 1970]), but these values cannot be compared to AWS 5 for which no cloud data are available.

[39] Turning to the ice shelf stations, AWS 4 has a higher albedo than Neumayer and Halley, resulting in lower values of summer SHW_{net} and R_{net}. Wintertime LW_{net} compares

Table 3. Mean Summer (December/January), Winter (July/August), and Annual Net Radiation Fluxes at the Four AWS and Other Antarctic Stations

			Summer			Winter			Year
	Period	α	SHW_{net}	LW_{net}	R_{net}	SHW_{net}	LW_{net}	R_{net}	R_{net}
Plateau									
AWS 9	1998–2001	0.85	70.6	−59.1	11.5	0.2	−13.1	−12.9	−6.9
South Pole	1986–1988	0.81	76.2	−60.0	15.2	0.0	−12.6	−12.6	NA
Vostok	1963–1973	0.83	72.8	−46.7	26.1	0.1	−16.8	−16.7	−2.8
Plateau[a]	1967	0.82	74.7	−61.8	12.9	0.1	−15.6	−15.5	−7.8
Inland katabatic									
AWS 6	1998–2001	0.84	60.6	−55.4	5.1	0.3	−36.8	−36.5	−22.1
Mizuho	1979–1980	0.78	82.7	−67.3	15.4	1.4	−33.0	−31.6	−13.3
Coastal katabatic									
AWS 5	1998–2001	0.84	54.5	−46.4	8.1	0.6	−28.9	−28.3	−15.6
Syowa	1987	0.74	81.5	−56.5	25.0	1.0	−44.0	−43.0	−17.9
Ice shelf									
AWS 4	1998–2001	0.88	42.9	−36.8	6.1	0.4	−16.0	−15.6	−7.0
Neumayer	1982–1992	0.82	54.5	−33.0	21.5	1.5	−18.5	−17.0	−5.3
Halley[a]	1963–1982	0.81	57.8	−43.9	13.9	0.4	−22.2	−21.9	−9.6

[a]Shortwave radiation and all-wave radiation were measured, and longwave radiation was calculated.

well between the stations and to those published for ice shelf station Maudheim (−21.3 W m^{-2} [*Liljequist*, 1957]). Annual mean R_{net} is small and negative at all three ice shelf stations, and is comparable to the values for the plateau stations. Note that the differences between AWS 4 and Neumayer are smaller if we compare data measured during the same period at both stations (Table 2).

[40] To summarize this section, we note that interannual as well as spatial variability is large in all components of the radiation balance. As a result, comparing station data from different periods must be done with care, and no firm conclusions on differences in radiation climatology can be derived from it. At most we can say that there is qualitative agreement between the radiation fluxes measured at the AWS and the manned stations listed here.

4.2. Albedo Variations

[41] Because of their good spatial and temporal coverage, AWS data could serve as a basis for parameterizations of Antarctic surface albedo in atmospheric models. For instance, an important result is that average surface albedo varies considerably in space and time (Figures 4 and 5b and Table 2), in spite of the apparently homogeneous Antarctic snow surface. In section 3.2.2 we could explain these variations qualitatively as a function of cloud cover, snow age and solar zenith angle. While average values lie between 0.84 and 0.88, values as high as 0.95 are observed during cloudy episodes with fresh snow. This means that atmospheric models that assume a constant albedo of 0.8 over Antarctica overestimate the instantaneous amount of absorbed shortwave radiation by 25–400%, which may well explain the warm summer bias that is present in many of these models.

[42] A parameterization of albedo would require multiple regressions incorporating solar zenith angle, snow age and cloud cover/diffuse fraction, and is outside the scope of this paper. As a first step toward such a parameterization, Figures 11a–11e show daily mean α_{acc} as a function of LW_{net} (which is a measure of cloudiness), for days with average zenith angles <85°. At all sites, cloud cover appears to be an important factor toward an explanation of temporal albedo variations. The similarity between the AWS and Neumayer supports the quality of the AWS radiation data.

[43] An interesting consequence of the strong correlation between cloud cover and albedo is that it partly offsets the warming effect that clouds usually have over highly reflective surfaces (the ''radiation paradox''). This effect also represents a negative feedback on Antarctic near-surface warming, when in an enhanced greenhouse scenario cloudiness in Antarctica is likely to increase [*van Lipzig et al.*, 2002].

4.3. Clear-Sky Longwave Emissivity

[44] Another application of the AWS radiation data is to study the location dependency of effective clear-sky emissivity, for instance for the parameterization of LW↓ as a function of near-surface temperature. These parameterizations can be used in energy balance and mass balance models of ice sheets [*Konzelmann et al.*, 1994; *van de Wal and Oerlemans*, 1997]. Figure 12a shows straight lines fitted through the origin and the 5th and 95th percentile of daily mean LW↓ at AWS 4 and 9, binned in 5 K temperature intervals. The 95th percentile should give a reliable sample of overcast days, the 5th percentile a good representation of clear days. We have added 10 W m^{-2} error bars as a typical spread of LW↓ in these temperature bins. Temperature on the *x*-axis is expressed as a radiative flux at unit emissivity, so that the slopes of the fits are equivalent to effective atmospheric emissivities ε_{eff}. The overcast data are well modelled by $\varepsilon_{eff} = 1$, with slopes of 1.007 ± 0.008 and 0.987 ± 0.012 at AWS 4 and 9, respectively. The clear-sky ε_{eff} have values of 0.760 ± 0.007 and 0.646 ± 0.010 at AWS 4 and 9, respectively. The clear-sky value of ε_{eff} at AWS 4 agrees well with the value of 0.765 found for Neumayer [*König-Langlo and Augstein*, 1994]. A similar exercise yields ε_{eff} = 0.675 ± 0.011 and 0.634 ± 0.008 for the effective clear-sky emissivities at AWS 5 and 6.

[45] The variation of ε_{eff} with station elevation is presented in Figure 12b. There are several competing effects that explain the differences in ε_{eff} between the stations. First, (saturation) atmospheric moisture content increases exponentially with temperature, so that LW↓ and hence ε_{eff} decrease strongly when moving from the coast inland. Second, the surface-based temperature inversions at AWS 4 and AWS 9 are stronger than in the katabatic wind zone [*van den Broeke et al.*, 2002]; surface temperatures are thus relatively low at these stations and higher values of ε_{eff} are needed to couple near-surface temperature to the effective radiating level in the upper atmosphere. This explains the increase of ε_{eff} onto the plateau.

5. Summary

[46] We presented 4 years of uninterrupted near-surface radiation observations from four Antarctic automatic weather stations (AWS). The AWS are situated along a traverse line in Dronning Maud Land, East Antarctica, connecting the coastal ice shelf to the high polar plateau via the katabatic wind zone. A direct comparison with radiation observations from manned stations supports the assumption that reliable radiation measurements can be made at unmanned platforms in Antarctica, although outside of the katabatic wind zone one must be wary of icing problems in winter. The main results are as follows:

[47] 1. Apart from shielding the surface from solar radiation and bringing fresh, highly reflective snow, clouds absorb near-infrared radiation. This strongly increases surface albedo and further reduces the amount of shortwave radiation that is absorbed at the surface.

[48] 2. As a result, significant albedo differences are found between the coastal ice shelf (α = 0.88), where clouds and precipitation events are frequent, and the coastal katabatic wind zone (α = 0.84), where accumulation events are less frequent.

[49] 3. The shortwave and longwave radiation balances are coupled, in the sense that more absorption of shortwave radiation leads to enhanced loss of longwave radiation. This limits the differences in summer net radiation among the stations.

[50] 4. Katabatic winds maintain a continuous turbulent transport of sensible heat toward the surface, which is balanced by enhanced outgoing longwave radiation. As a result, stations in the katabatic wind zone show the largest

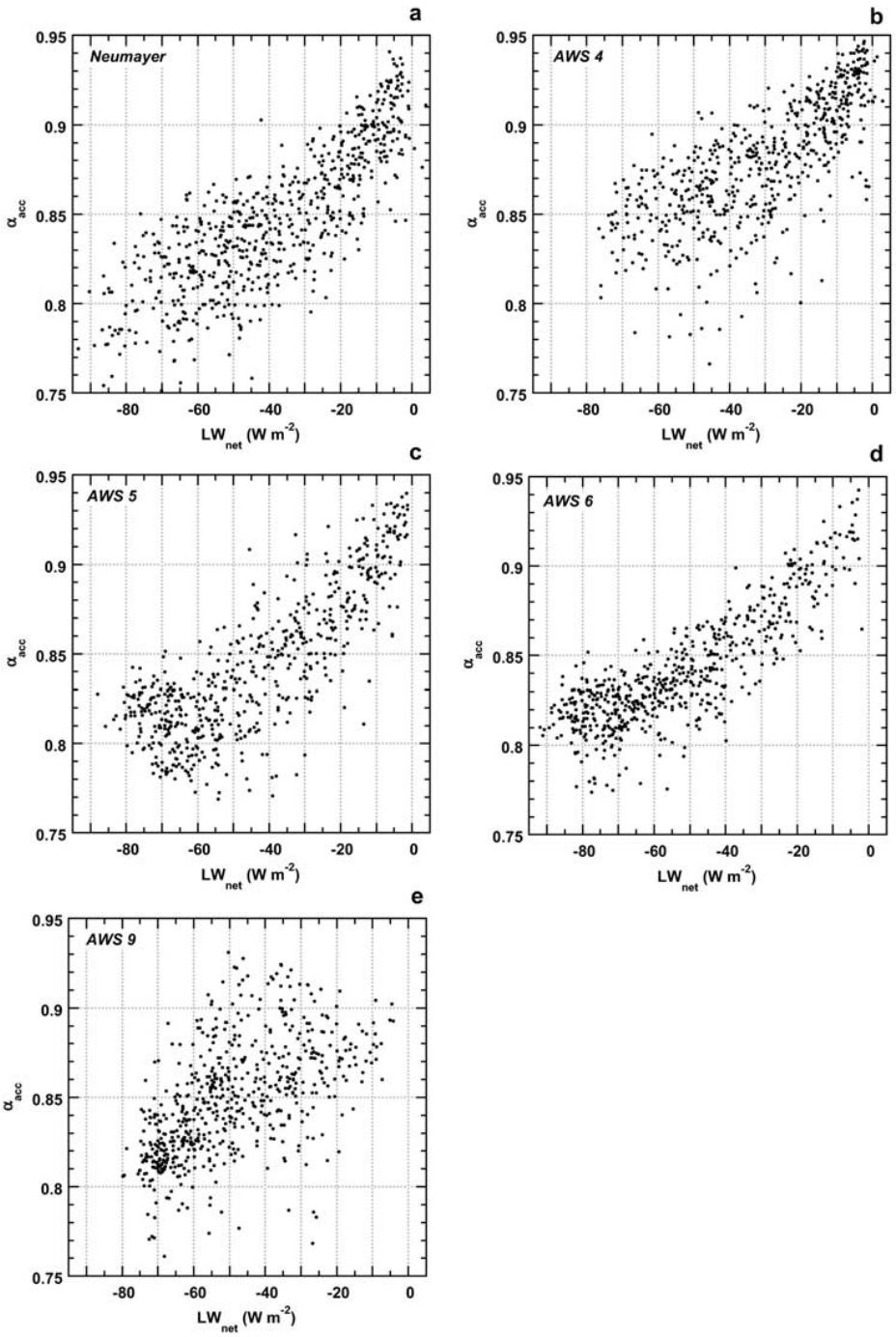

Figure 11. Daily mean accumulated albedo α_{acc} as a function of net longwave radiation at (a) Neumayer, (b) AWS 4, (c) AWS 5, (d) AWS 6, and (e) AWS 9. Only days are included where average zenith angle <85°.

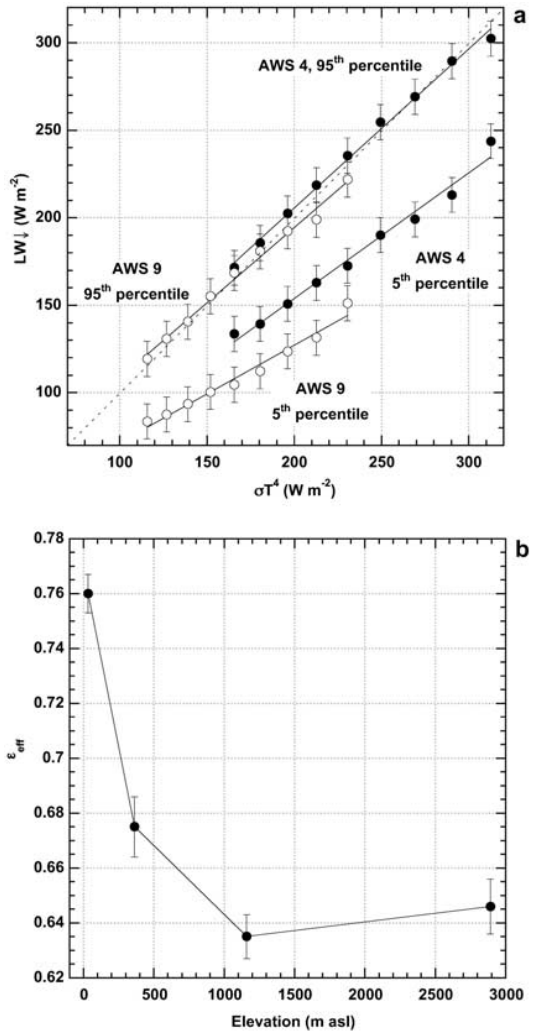

Figure 12. (a) Linear fits to the 5th and 95th percentiles of incoming longwave radiation, binned in 5 K temperature intervals, as a function of AWS temperature (expressed as a radiation flux) for AWS 4 (solid circles) and AWS 9 (open circles). The 1:1 line is dashed. (b) Clear-sky emissivity as a function station elevation.

all-wave/longwave radiation loss in winter as well as over the year.

[51] 5. In regions where katabatic winds are moderate and accumulation sufficiently frequent, the surface albedo remains high; this is where the annual net radiation loss is greatest (< -20 W m^{-2}).

[52] 6. Clear-sky effective emissivity for incoming longwave radiation shows great spatial variability resulting from differences in vertical temperature and moisture profiles among the various climate zones.

[53] **Acknowledgments.** We thank the technical department of IMAU for designing, building and maintenance of the AWS. Participants of SWEDARP'97/98 are thanked for setting up AWS 4, 5 and 6. Field parties of IMAU are thanked for maintenance work on AWS 4, 5 and 6, and personnel of the Alfred Wegener Institut are thanked for the setting up and maintenance of AWS 9. This work is partly funded by the Netherlands Antarctic Program (NAAP) and the Netherlands Organisation of Scientific Research, section Earth and Life Sciences (NWO/ALW). This work is also a contribution to the "European Project for Ice Coring in Antarctica" (EPICA), a joint ESF (European Science Foundation)/EC scientific programme, funded by the European Commission and by national contributions from Belgium, Denmark, France, Germany, Italy, Netherlands, Norway, Sweden, Switzerland, and the United Kingdom. This is EPICA publication 96.

References

Allison, I., G. Wendler, and U. Radok (1993), Climatology of the East Antarctic ice sheet (100°E to 140°E) derived from automatic weather stations, *J. Geophys. Res.*, *98*(D5), 8815–8823.

Bintanja, R. (2000), Surface heat budget of Antarctic snow and blue ice: Interpretation of spatial and temporal variability, *J. Geophys. Res.*, *105*(D19), 24,387–24,408.

Bintanja, R., and M. R. van den Broeke (1995), The surface energy balance of Antarctic snow and blue ice, *J. Appl. Meteorol.*, *34*, 902–926.

Bromwich, D. H. (1989), Satellite analyses of Antarctic katabatic wind behavior, *Bull. Am. Meteorol. Soc.*, *70*, 738–749.

Carroll, J. J., and B. W. Fitch (1981), Effects of solar elevation and cloudiness on snow albedo at the South Pole, *J. Geophys. Res.*, *86*(C6), 5271–5276.

Colbeck, S. C. (1975), Grain and bond growth in wet snow, in *Snow Mechanics Symposium*, *IAHS AISH Publ.*, *114*, 51–61.

Dutton, E. G., R. S. Stone, D. W. Nelson, and B. G. Mendonca (1991), Recent interannual variations in solar radiation, cloudiness and surface temperature at the South Pole, *J. Clim.*, *4*, 848–858.

Fujii, Y., and Y. Kusunoki (1982), The role of sublimation and condensation in the formation of ice sheet surface at Mizuho station, Antarctica, *J. Geophys. Res.*, *87*(C6), 4293–4300.

Gay, M., M. Fily, C. Genthon, M. Frezzotti, H. Oerter, and J.-G. Winther (2002), Snow grain-size measurements in Antarctica, *J. Glaciol.*, *48*(163), 527–535.

King, J. C. (1996), Longwave atmospheric radiation over Antarctica, *Antarct. Sci.*, *8*, 105–109.

King, J. C., and W. M. Connolley (1997), Validation of the surface energy balance over the Antarctic ice sheets in the UK Meteorological Office Unified Climate Model, *J. Clim.*, *10*, 1273–1287.

King, J. C., and J. Turner (1997), *Antarctic Meteorology and Climatology*, *Cambridge Atmos. Space Sci. Ser.*, 409 pp., Cambridge Univ. Press, New York.

King, J. C., S. D. Mobbs, J. M. Rees, P. S. Anderson, and A. D. Cliff (1989), The STABLE Antarctic boundary layer experiment at Halley station, *Weather*, *44*, 398–405.

King, J. C., M. J. Varley, and T. A. Lachlan-Cope (1998), Using satellite thermal infrared imagery to study boundary-layer structure in an Antarctic katabatic wind region, *Int. J. Remote Sens.*, *19*, 3335–3348.

König-Langlo, G., and E. Augstein (1994), Parameterisation of the downward long-wave radiation at the Earth's surface in polar regions, *Meteorol. Z.*, *3*(6), 343–347.

Konzelmann, T., R. S. W. van de Wal, W. Greuell, R. Bintanja, A. A. C. Henneken, and A. Abe-Ouchi (1994), Parameterisation of global and longwave incoming radiation for the Greenland ice sheet, *Global Planet. Change*, *9*, 143–164.

Kuhn, M., L. S. Kundla, and L. A. Strohschein (1977), The radiation budget at Plateau Station, Antarctica, in *Meteorological Studies at Plateau Station*, *Antarct. Res. Ser.*, vol. 25, edited by J. A. Businger, pp. 41–73, AGU, Washington, D. C.

Liljequist, G. H. (1957), Energy exchange over an Antarctic snow field: Long-wave radiation and radiation balance (Maudheim), *Norwegian, British, Swedish Antarctic Expedition, 1949–1952: Scientific Results*, vol. 2, part 1b, Norsk Polarinst., Oslo.

Ohata, T., S. Kobayashi, N. Ishikawa, and S. Kawaguchi (1985a), Heat balance at the snow surface in a katabatic wind zone, East Antarctica, *Ann. Glaciol.*, *6*, 174–177.

Ohata, T., S. Kobayashi, N. Ishikawa, and S. Kawaguchi (1985b), Structure of the katabatic winds at Mizuho station, East Antarctica, *J. Geophys. Res.*, *90*(D6), 10,651–10,658.

Ohmura, A., et al. (1998), Baseline Surface Radiation Network (BSRN/WRMC), a new precision radiometry for climate research, *Bull. Am. Meteorol. Soc.*, *79*, 2115–2136.

Reijmer, C. H. (2001), Antarctic meteorology: A study with automatic weather stations, Ph.D. thesis, 158 pp., Utrecht Univ., Utrecht, Netherlands.

Reijmer, C. H., and J. Oerlemans (2002), Temporal and spatial variability of the surface energy balance in Dronning Maud Land, East Antarctica, *J. Geophys. Res.*, *107*(D24), 4759, doi:10.1029/2000JD000110.

Reijmer, C. H., and M. R. van den Broeke (2004), Accumulation in Dronning Maud Land, Antarctica, *J. Glaciol.*, in press.

Renfrew, I. A., and P. S. Anderson (2002), The surface climatology of an ordinary katabatic wind regime in Coats Land, Antarctica, *Tellus*, *Ser. A*, *54*, 464–484.

Schlatter, T. W. (1972), The local surface energy balance and subsurface temperature regime in Antarctica, *J. Appl. Meteorol.*, *11*, 1048–1062.

Schwerdtfeger, W. (1970), The climate of the Antarctic, in *World Survey of Climatology*, vol. 14, *Climates of the Polar Regions*, edited by S. Orvig, chap. 4, pp. 253–355, Elsevier Sci., New York.

Stanhill, G., and S. Cohen (1997), Recent changes in solar irradiance in Antarctica, *J. Clim.*, *10*, 1078–2086.

Stearns, C. R., and G. Wendler (1988), Research results from Antarctic automatic weather stations, *Rev. Geophys.*, *26*(1), 45–61.

Stearns, C. R., L. M. Keller, G. A. Weidner, and M. Sievers (1993), Monthly mean climatic data for Antarctic automatic weather stations, in *Antarctic Meteorology and Climatology, Studies Based on Automatic Weather Stations*, *Antarct. Res. Ser.*, vol. 61, edited by D. H. Bromwich and C. R. Stearns, pp. 1–21, AGU, Washington, D. C.

Streten, N. A. (1990), A review of the climate of Mawson: A representative strong wind site in East Antarctica, *Antarct. Sci.*, *2*, 79–89.

van den Broeke, M. R., J.-G. Winther, E. Isaksson, J. F. Pinglot, L. Karlöf, T. Eiken, and L. Conrads (1999), Climate variables along a traverse line in Dronning Maud Land, East Antarctica, *J. Glaciol.*, *45*, 295–302.

van den Broeke, M. R., N. P. M. van Lipzig, and E. van Meijgaard (2002), Momentum budget of the East-Antarctic atmospheric boundary layer: Results of a regional climate model, *J. Atmos. Sci.*, *59*, 3117–3129.

van den Broeke, M. R., D. van As, C. H. Reijmer, and R. S. W. van de Wal (2004b), Assessing and improving the quality of unmanned radiation observations in Antarctica, *J. Atmos. Oceanic Technol.*, in press.

van de Wal, R. S. W., and J. Oerlemans (1997), Modelling the short-term response of the Greenland ice sheet to global warming, *Clim. Dyn.*, *13*, 733–744.

van Lipzig, N. P. M., E. van Meijgaard, and J. Oerlemans (2002), Temperature sensitivity of the Antarctic surface mass balance in a regional atmospheric climate model, *J. Clim.*, *15*, 2758–2774.

Vaughan, D. G., and C. S. M. Doake (1996), Recent atmospheric warming and retreat of ice shelves on the Antarctic Peninsula, *Nature*, *379*, 328–331.

Walden, V. P., S. G. Warren, and F. J. Murcray (1998), Measurements of the downward longwave radiation spectrum over the Antarctic plateau and comparisons with a line-by-line radiative transfer model for clear skies, *J. Geophys. Res.*, *103*(D4), 3825–3846.

Weller, G. (1981), Spatial and temporal variations in the South Pole energy balance, *Mon. Weather Rev.*, *108*, 2006–2014.

Wendler, G., N. Ishikawa, and Y. Kodama (1988), The heat balance of the icy slope of Adélie Land, Eastern Antarctica, *J. Appl. Meteorol.*, *27*, 52–65.

Wiscombe, W. J., and S. G. Warren (1980), A model for the spectral albedo of snow: I: Pure snow, *J. Atmos. Sci.*, *37*, 2712–2733.

Yamanouchi, T., and J. B. Ørbaek (1995), Comparative study of the surface radiation budget at Ny-Ålesund, Svalbard and Syowa Station, Antarctica, 1987, *Proc. NIPR Symp. Polar Meteorol. Glaciol.*, *9*, 118–132.

C. Reijmer, M. van den Broeke, and R. van de Wal, Institute for Marine and Atmospheric Research, Utrecht University, P. O. Box 80005, 3508TA Utrecht, Netherlands. (broeke@phys.uu.nl)

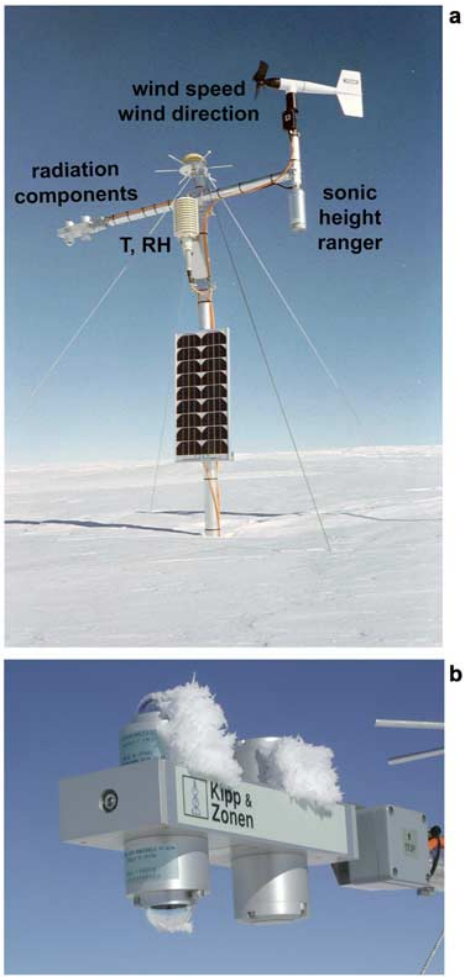

Figure 2. (a) Picture of AWS 9, taken 4 years after installation, i.e., after approximately 1 m of snow has accumulated. The datalogger and pressure sensor are buried in the snow. The other AWS have similar designs. (b) Enlargement of radiation sensor with ice accretion.